NeuroImage 331 (2026) 121870

Contents lists available at ScienceDirect

NeuroImage

journal homepage: www.elsevier.com/locate/ynimg

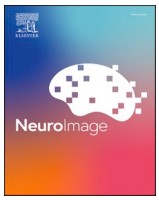

Multimodal MRI of the reorganization of multisensory and sensorimotor networks in chronic bilateral vestibulopathy

Marianne Dieterich [a,b,c,1,*], Thomas Stephan [a,b,1], Lena Fabritius [a,b], Rainer Boegle [a,b,1], Thomas Brandt [a,1]

[a] German Center for Vertigo and Balance Disorders, LMU University Hospital, LMU Munich, Munich, Germany
[b] Department of Neurology, LMU University Hospital, LMU Munich, Munich, Germany
[c] Munich Cluster for Systems Neurology (SyNergy), Munich, Germany

ARTICLE INFO

Keywords:
Multimodal imaging
Visual-vestibular interaction
Compensation
Bilateral vestibulopathy
Hippocampus
Prefrontal cortex
Voxel-based morphometry
Connectivity
Sensorimotor networks

ABSTRACT

Chronic bilateral vestibulopathy (BVP) occurs preferably in elderly patients presenting with postural imbalance and head movement induced oscillopsia. The condition is often incomplete with residual functions in both ears. Beyond the vestibular reflexive deficits, an impairment of spatial orientation and navigation has been described associated with an atrophy of the hippocampal formation. However, this finding was inconsistent in various studies on rodents and humans. In the current MRI study on 15 BVP patients and 15 healthy controls (HC) we combined analyses of whole brain voxel-based morphometry (VBM) and the resting state fMRI (rs-fMRI) on the widely distributed multisensory vestibular network and its connections to sensorimotor, cognitive, and emotional networks at rest. Major results were gray and white matter changes in conjunction with rs-fMRI changes: the left posterior insula, angular and supramarginal gyri, and left premotor cortex; as well as bilateral anterior hippocampal formation and adjacent amygdala; visual cortex V1 and V5; thalamus; prefrontal cortex; cerebellar hemispheres and uvula; and pyramidal tract. Thus, the overlap of structural (VBM) and rs-fMRI including various correlation analyses disclosed that a bilateral reduction of peripheral vestibular input affects multiple networks from the cerebellum up to the cortical hemispheres. A possible functional interpretation is that the observed specific alterations reflect compensation and substitution by other networks – handling perception, sensorimotor balance regulation, cognition, and emotions - due to deficits in one sensory system. This is consistent with anterior hippocampal atrophy's role in spatial memory deficits, as well as the involvement of the cerebellum, amygdala, and prefrontal cortex in emotional processes. It also aligns with the top-down regulation by the prefrontal cortex via the pyramidal tract for cognitive control of balance triggered by the perception of postural instability. Further, correlation analyses support this interpretation because most morphological changes were dependent on the duration of the condition.

1. Introduction

Chronic bilateral peripheral vestibular loss, also referred to as bilateral vestibulopathy (BVP), is a well recognized and defined diagnosis in a tertiary interdisciplinary center for vertigo and balance disorders accounting for 6.2% of the patients (Strupp et al., 2023). Clinically it presents primarily with symptoms such as imbalance in posture and gait, especially on uneven surfaces, in darkness, and with head-movement often leading to oscillopsia. The current diagnostic criteria for BVP and probable BVP have been defined by the Classification Committee of the Bárány Society (Strupp et al., 2017). The deficit of both labyrinths or peripheral nerves may develop simultaneously or sequentially and is often incomplete with residual functions in one or both ears. Beyond the typical reflexive deficits of vestibulo-spinal and ocular motor control, an impairment of spatial orientation, spatial memory and navigation has been described in animals (Smith et al., 2005; Zheng et al., 2009; Smith et al., 2015) and humans with complete (Brandt et al., 2005) and incomplete BVP (Göttlich et al., 2016; Kremmyda et al., 2016; Smith, 2024) and even temporarily in acute unilateral vestibulopathy (Oh et al., 2023, 2025).

* Corresponding author at: German Center for Vertigo and Balance Disorders, LMU University Hospital, Munich, Marchioninistrasse 15, 81377 München, Germany.
E-mail address: Marianne.Dieterich@med.uni-muenchen.de (M. Dieterich).
[1] Equal contribution.

https://doi.org/10.1016/j.neuroimage.2026.121870
Received 1 August 2025; Received in revised form 25 November 2025; Accepted 20 March 2026
Available online 20 March 2026

Moreover, cognitive deficits beyond spatial orientation were discussed (Popp et al., 2017; Dobbels et al., 2019; Bosmans et al., 2022). First imaging studies on complete bilateral vestibular loss revealed an associated atrophy of the hippocampal formation (Brandt et al., 2005) which appeared less pronounced in patients with incomplete BVP (Kremmyda et al., 2016). However, other studies did not find volume decreases of the hippocampus in particular when vestibular loss was incomplete (rat: Zheng et al., 2012; humans: Dordevic et al., 2021; Bosmans et al., 2024). Since the findings on hippocampal volume were inconsistent, further studies also focused primarily on the gray matter volume of the hippocampal complex, for example describing a volume reduction in the bilateral hippocampal CA3 region which could only be detected through its correlation with the severity of clinical impairment caused by BVP (Göttlich et al., 2016).

While earlier studies focused on the hippocampal structures, there remains a lack of understanding regarding changes in other cortical areas of the widespread central vestibular network, which reaches from the brainstem and cerebellum all the way to the temporo-parieto-insular cortex - the so-called vestibular core region - and the frontal lobes (meta-analyses: Lopez et al., 2012; zu Eulenburg et al., 2012; Neumann et al., 2023). There is only one study in BVP patients on functional and anatomical alterations examining the entire brain including voxel-based morphometry decreases in a few extrainsular areas and the posterior hippocampus (Lee et al., 2023). In the latter study, the emphasis was on functional connectivity without discussion of any associated volume changes in the vestibular insular region. Furthermore, there is evidence of an interaction of the vestibular and the anxiety networks. Clinical data and meta-analytic imaging data suggested a considerable overlap between vestibular-sensory and anxiety-emotional processing networks (Neumann et al., 2023; Lotze et al., 2025). Thus, the latter studies revealed functional associations between vestibular insular fMRI activity and trait anxiety.

In the current MRI study in BVP patients we combined whole brain voxel-based morphometry and functional connectivity analyses on the multisensory network and its connections to cognitive, emotional and association networks at rest. Analyses of the data included correlations to the duration and severity of the disease, as well as trait anxiety scores. Two groups of participants were enrolled, patients with chronic incomplete BVP and age- and sex-matched healthy controls. In essence, the goal was to determine whether this methodological approach is suitable for explaining the reorganization of multisensory and sensorimotor control that the system undergoes in order to substitute or compensate for the missing vestibular input. This would most likely manifest as a potential modification of the volumes of sensorimotor areas and the connectivity of the vestibular network with other sensory, sensorimotor, and emotional networks processed by ascending and descending pathways.

2. Methods

This prospective study was conducted in the interdisciplinary outpatient clinic of the German Center for Vertigo and Balance Disorders at LMU University Hospital, Munich, Germany. All participants provided their written informed consent in accordance with the Declaration of Helsinki and its later amendments before inclusion in the study, which was approved by the Ethics Committee of the LMU University

Table 1
Pertinent demographic, clinical and diagnostic features in 15 patients with BVP.

No	Sex F/M	Age	Duration*	Symptoms	Calorics (WR/CR–WL/CL)	vHIT (R/L)	Disease Score	STAI State - Trait	Etiology
1	M	68	3 y	Persistent dizziness, oscillopsia while walking, hypacusis left after gentamicin; bilateral tinnitus, hearing loss L>R; before that 3 MD attacks left	3.8/0.6–2.3/1.3	0.99/0.48	7	45 - 38	MD with gentamicin left ear, ototoxic
2	M	68	2 y	Persistent imbalance of stance and gait, oscillopsia during movements, bilateral high frequency hearing loss	3.7/2.0–0.6/4.7	0.19/0.59	10	51 - 44	Unclear
3	M	37	8 y	Persistent dizziness and oscillopsia during gait, hypacusis right	1.4/4.2—6.1/7.8	0.15/0.53	8	65 - 55	Unclear
4	F	77	23 y	Persistent gait instability, oscillopsia, bilateral visual deficits	1.6/0.8—2.8/0.5	0.15/0.13	14	26 - 35	Autoimmune, Sjögren
5	M	39	1.5 y	After inflammation of the middle ear and azithromycin continuous gait instability and oscillopsia, no hearing loss	0.1/1.5–0.3/1.4	0.25/0.37	13	23 - 29	Ototoxic, aminoglycoside
6	F	67	4 y	Imbalance of stance and gait	0/1.7—1.3/0	0.17/0.23	15	44 - 42	Unclear
7	M	63	14 mths	3 attacks of vertigo and oscillopsia for 30 s, thereafter ongoing oscillopsia and gait imbalance, that improved after corticosteroids	3.3/0.6—0.4/2.0	0.63/0.51	9	51 - 37	Unclear, autoimmune?
8	F	68	2.5 y	Slowly increasing gait imbalance	3.2/2.1—0.9/1.0	0.69/0.38	10	51 - 42	Unclear
9	F	40	8 y	8 y ago acute vestibular neuritis left, thereafter fluctuating dizziness and oscillopsia, bilateral tinnitus slowly improving; vestibular neuritis right 11 y ago	2.9/1.1—0/2.4	0.71/0.45	9	33 - 33	Autoimmune
10	M	52	2.75 y	Attacks of double vision and wobbling of the horizon for 5 min every 2 months, persistent oscillopsia during movements, gait imbalance in the dark	5.7/0—0.1/4.1	0.46/0.35	9	41 - 30	Unclear
11	M	64	1.5 y	Dizziness and gait imbalance persistent after gentamicin due to endocarditis, no hearing loss	1.9/0—0.7/0.4	0.36/0.26	14	33 - 29	Ototoxic, gentamicin
12	M	59	4 y	Persisting dizziness during walking, gait imbalance, brief vertigo attacks before	1.5/0.6—0.3/1.4	0.04/0.44	13	30 - 41	Unclear
13	F	56	6 y	Increasing gait imbalance and oscillopsia during movements, increasing hearing loss left>right	0.2/0.6—0.2/0.2	0.16/0.05	16	35 - 43	Unclear
14	F	69	5 y	Slowly increasing gait imbalance	0.3/6.0—0.9/0.5	0.14/0.36	12	52 - 48	Unclear
15	M	70	5 mths	Gait imbalance after treatment of endocarditis with vancomycin and gentamicin	0.3/3.5—3.3/0.1	0.33/0.23	12	24 - 38	Ototoxic, aminoglycosides

Duration*: duration of BVP symptoms.
Abbreviations: Y= year; mths= months; MD= Ménière's Disease; s= seconds; Calorics (nystagmus of slow phase in degrees per second): WR= warm right, CR= cold right, WL= warm left, CL= cold left; STAI = State Trait Anxiety Inventory, vHIT= video head impulse test.

Hospital (reference number: 108-10).

2.1. Participants

All patients received a detailed neurological and neuro-otological workup with an extensive neuro-orthoptic examination (Table 1). This included bithermal water caloric testing (for the function of the horizontal semicircular canals in the low-frequency range of the vestibulo-ocular reflex; velocity of the slow nystagmus phase) (Jongkees et al., 1962) and standardized video-head impulse test (vHIT) measurements of the semicircular canal function in the high-frequency range using the EyeSeeCamHIT system (EyeSeeTeec, Munich, Germany) (Halmagyi et al., 2017). Furthermore, pure tone audiometry, and a comprehensive neuro-orthoptic examination with ocular motor and visual acuity testing, assessment of the subjective visual vertical, and fundus photography to determine the signs of an acute vestibular graviceptive dysfunction and vestibular tone imbalance in the roll plane were performed (for details see: Strupp et al., 2023). Posturographic measurements (stabilometer platform; Kistler 9261A; Kistler Group, Winterthur, Switzerland), gait analyses, ocular and cervical vestibulo-myogenic potentials (VEMPs), and neurography of peripheral nerves were added, if clinically useful. All patients received cranial MRI during the diagnostic process in standardized manner to exclude concurring structural pathologies. All participants were tested for handedness by using the Edinburgh Handedness Inventory (Oldfield, 1971).

The assessment of disease scores involved the two primary tests: the vHIT and the caloric test. The scoring system for the vHIT was as follows: normal result: 0 points, borderline gain (0.61 - 0.8): 1 point, moderate impairment (0.41 - 0.6): 2 points, severe impairment (0.21 - 0.4): 3 points, profound impairment (0 - 0.2): 4 points. For caloric test evaluation the key parameter measured was the slow phase velocity (in degrees per second) of caloric nystagmus, which was summed for bithermal stimulation of each ear. The scoring criteria were: normal response: 0 points, moderate response (6.1 - 8.0 °/s): 1 point, mild response (4.1 - 6.0 °/s): 2 points, significant reduction of response (2.1 - 4.0 °/s): 3 points, minimal or absent response (0 - 2.0 °/s): 4 points. Overall, the scores for vHIT and for caloric irrigation with both temperatures were added together for both ears, resulting in a total value of 16 points at maximum damage (4 × 4 points: vHIT right + vHIT left + bithermal calorics right + bithermal calorics left).

All neurological diagnoses were made according to the diagnostic criteria of the Bárány Society for bilateral vestibulopathy (BVP) (https://www.thebaranysociety.org/icvd-consensus-documents) and their precursors (Strupp et al., 2017; Halmagyi et al., 2017; Jongkees et al., 1962). Additionally, the patients had to fill out the State-Trait-Anxiety Inventory (STAI-T)(Laux et al., 1981).

In the current study, 15 BVP patients and 15 age- and gender-matched healthy controls (HC) with normal vestibular testing were enrolled (Table 1).

2.2. Imaging data acquisition

Imaging data was acquired on a 3 Tesla MRI scanner (Siemens Skyra), using a 64-channel head coil. From every subject, a high-resolution T1 weighted structural scan was acquired (isotropic voxel size of 0.75 mm) using an MPRAGE sequence. Resting-state functional MRI (rs-fMRI) data were recorded using a multiband echo-planar imaging sequence (685 EPI volumes, 64 × 64 × 54 isotropic voxels, voxel size 2.5 mm, TR 700 ms, multiband factor 6, TE 33 ms) in axial orientation and aligned to the AC-PC plane. Subjects had their eyes open with a visual fixation target during RS-fMRI data acquisition.

2.3. VBM imaging data analysis

2.3.1. VBM data preprocessing

Voxel based morphometry (VBM) of the T1 weighted structural images was used to analyze the local volumes of gray matter (GM) and white matter (WM). Data was processed using the CAT12 toolbox version 2170 (Gaser et al., 2024) within the framework of SPM12 (version 7771, https://www.fil.ion.ucl.ac.uk/spm/). Images were segmented into compartments of GM and WM, and normalized into MNI standard space using DARTEL with geodesic shooting (Ashburner 2007). The segmented compartment images were smoothed with an isotropic Gaussian kernel (FWHM 8mm).

2.3.2. VBM statistical analysis

Two different General Linear Models (GLM) were used within SPM to test for volume changes in whole brain voxel-wise statistical analysis. To test for differences between patients and controls, we implemented a two-sample t-test that additionally accounted for total intracranial volume, age, sex, and trait-anxiety (TRAX). Group differences were assessed using linear contrasts (PAT vs. NP, NP vs. PAT). A second GLM (one-sample t-test with covariates) was used to test for changes associated with disease duration, BVP-score, and trait-anxiety (TRAX), while accounting for age, sex, and total intracranial volume. All statistical tests were replicated for GM and WM in separate analyses. Results were thresholded at $p<0.001$ (uncorrected) and a minimum cluster size of 100 voxels. To provide additional labels for areas in frontopolar and prefrontal regions, the parcellation according to Schaefer (400 parcels, 17 Networks) was used (Schaefer et al., 2018, Yeo et al., 2011).

2.4. Resting state functional imaging (rs-fMRI) data analysis

2.4.1. Preprocessing of rs-fMRI data

The first 30 image volumes from the resting-state time series were deleted to avoid T1 saturation effects. Preprocessing of the data was performed using SPM12 and included correction for head motion by realignment, coregistration to the individual high-resolution T1 scan, spatial normalization into MNI space by application of the warping parameters that were obtained during VBM data processing (see above), and smoothing with an isotropic Gaussian kernel (FWHM 4 mm).

2.4.2. Independent component analysis for denoising of rs-fMRI data

Resting-state fMRI (rs-fMRI) data was denoised using a group independent component analysis (gICA) combined with dual regression approach we have used in previous studies (Cyran et al., 2016; Kirsch et al., 2018). High-dimensional gICA with 350 dimensions followed by dual-regression to generate individual contributions per subject was used to distinguish noise and signal sources in the fMRI data from both groups, using FSL-MELODIC version 3.15 (Beckmann and Smith, 2004; Nickerson et al., 2017). Components that were judged to be noise were removed from the signal of each respective subject.

2.4.3. Measures of rs-fMRI fluctuations

Here we were interested in examining how signal properties of rs-fMRI data, in this work referred to as “rs-fMRI fluctuation measures”, change with disease status relative to HCs. However, the wide variety of measures of rs-fMRI fluctuations available, and the lack of an internationally accepted gold standard for measuring rs-fMRI fluctuations, led us to analyse a wide variety of measures in combination and report the pattern changes.

Before applying the measures of rs-fMRI fluctuations listed below (and explained in more detail in the supplementary methods), bandpass filtering between 0.143Hz and 0.007Hz was applied. This means signal periods of length 7s (10 TRs) to periods of 140s, (200 TRs) were included to limit high-frequency noise like pulsation and low-frequency influences like slow signal drifts.

All the following rs-fMRI fluctuation measures were used:

Amplitude of low-frequency fluctuations (ALFF) (Zang et al., 2007; Yang et al., 2007) measures the mean power-spectrum magnitudes of fluctuations (frequency domain without phase). Values were always positive with higher values indicating larger amplitudes in the frequency

range of interest on average.

Fractional ALFF (fALFF), a later extension (Zou et al., 2008), measures the fraction of the ALFF in the frequency range of interest compared to the full spectrum. Values range from 0 to 1, with larger values meaning higher average amplitudes in the frequency range of interest compared to the full frequency range of the signal.

Percent amplitude fluctuation (PAF) (Jia et al., 2020) is a time domain measure of absolute fluctuations around the mean and scaled by the timely mean amplitude, hence, akin to percent signal change in task fMRI. Its values were always positive and larger values indicate larger amplitudes in the rs-fMRI signal.

Furthermore, normalized versions of PAF were used:

1. mPAF was normalized to the spatial mean PAF (global signal). Hence always positive and values beyond 1 indicate fluctuations above the global signal, while values below 1 indicate fluctuations below the global signal.
2. zPAF was relative to the spatial mean PAF (global signal) and scaled by the spatial standard deviation of PAF (global signal variation). Therefore, values were relative to the global signal and scaled to the global signal variations. Negative values indicate fluctuations below the global signal, while positive values indicate fluctuations above the global signal, scaled by the variation of the global signal.

The mean squared successive difference (MSSD) and the median absolute successive difference (MASD) over time (von Neumann et al., 1941) were used as measures of general low-level variability of the signal. MSSD is strongly influenced by large deviations, while MASD is not; both measures are complementary, with both being positive and larger values indicating more variability between neighboring time steps on average.

Sample entropy (SaEn) was used to quantify signal complexity in an information theoretic sense, i.e., measuring the conditional probability that sequences of m consecutive time points remain similar (within tolerance r) to sequences of length m+1. SaEn was positive valued with lower values indicating higher signal regularity, while higher values reflect greater complexity or unpredictability (Richman and Moorman, 2000). We use pattern length m=4 and tolerance factor of r=0.3 (of time course standard deviation). Note that previous studies often used m=2, for fMRI sequences with TR of 2 seconds or longer, while we use m=4 with TR of 0.7 seconds (fast rsfMRI) to stay comparable to previous studies (e.g., compare with Yang et al., 2014; Sokunbi, 2014; Guan et al., 2023).

Regional homogeneity (ReHo) was used to measure the similarity of time courses between neighboring voxels (for each voxel and its 26 nearest neighbors). ReHo was measured via coherence in the frequency domain, ignoring phase differences (Liu et al., 2010), an extension of the time domain measure (Zang et al., 2004). ReHo values were positive and larger values indicate greater similarity or synchronization of neighboring voxels.

Voxel degree (VoxDeg) was used to measure the connectedness of each voxel to the rest of the brain, following the approach by Göttlich and co-workers (Göttlich et al., 2014). The time course of a voxel was correlated with time courses of all other voxels in the brain. Then the number of connected voxels after thresholding (absolute correlations greater than 0.25) was counted. The counts of connections were then z-transformed, i.e., relative to the mean number of connections and scaled by the standard deviation hence the variability of connections in the brain. Values larger than zero mean more connections than the average voxel and values lower than zero mean fewer connections than the average voxel.

2.4.4. Normalization of rs-fMRI fluctuation measures per voxel over both groups

Given that we wanted to perform statistical analysis using all rs-fMRI fluctuation measures together, it was necessary to normalize the values of all measures. For example, fALFF or ReHo values are between 0 and 1, while ALFF and PAF might be between 0 and 10, MSSD and MASD might be several 10^{th} or 100, and voxel degree or zPAF might be +-2 to +-4 in magnitude. For the residuals in a GLM-SPM model, this would imply for an assumed 10% error that residual fALFF would be on the order of 0.1, residual PAF could be on the order of 1 and residual MSSD might be on the order of 10. Therefore, the error of MSSD even if of a similar percentage of magnitude would dominate the residual mean squares. If tested individually this would not matter, but we wanted to create an omnibus test considering all measures.

Therefore, we normalized the values of all rs-fMRI fluctuation measures over all participants of the two groups by dividing the values of each participant, at each voxel, by the 95% quantile value of the absolute values of all participants and finally multiplying each value by 100. Therefore, all fluctuation measure values will kept their relative difference between groups but were transformed onto the same scale. Inspection of normed data at various locations showed that all transformations resulted in linear change of scale, with almost all data ranged between ±100 (some between ±120 and a few cases between ±200). Thus, this transformation ensured that all data kept their distribution and were on the same scale which makes assessment of all measures with one big SPM model and an omnibus F-test possible.

2.4.5. Statistical analysis of normed fluctuation measures

Analog to the VBM analysis, two types of models were created in SPM12, using all normed rs-fMRI fluctuation measures; one model testing the group differences between BVP and HC, and one model testing the covariate correlations. These covariates were the BVP disease duration, BVP-score, and trait-anxiety (TRAX), while accounting for age and sex. In each model the design matrix had block structure, i.e., each normed rs-fMRI fluctuation measure had its own sub-design matrix. The main test we were interested in was the omnibus test for each of the models, i.e., “Is there a group difference test for any amplitude measure?” or in the correlation case, “Is there a correlation for the covariate of interest for any fluctuation measure?”. This means that an F-test was constructed with each normed amplitude fluctuation measure tested by itself and all of these combined in a contrast-weights matrix in SPM.

This design matrix and F-tests allowed us to create overview statistical maps with all effects. Clusters were assessed via contrast-estimates for the individual contributions to the test difference by each normed amplitude fluctuation measure. The contrast-estimate also revealed the result direction and was then transferred into the overview statistical map. Thus, we could show the group differences and correlations including their directions in the omnibus statistical maps. Thresholding was done with family-wise error correction and threshold p=0.05/nFM, where nFM is the number of rs-fMRI fluctuation measures (10), and a minimum cluster size of 18 voxels (e.g., for a central voxel with its the closest neighbors in 2mm rs-fMRI resolution this would be a cube of $36mm^3$).

2.5. Analysis of overlaps between VBM and rs-fMRI results

To show close relations, but also differences, between VBM and rs-fMRI result maps, overlaps between result maps were created. The comparisons were done between correlations in both modalities (e.g., BVP disease duration results for VBM and rs-fMRI analysis) but also the group differences (e.g., BVP disease duration results for rs-fMRI analysis and VBM group differences). Overlaps were only considered if overlaps between maps were at least 64 voxels (e.g., a cube of 4 × 4 × 4 voxels).

3. Results

3.1. Patients

Clinical characteristics and results of vestibular function tests of the 15 right-handed BVP patients (6 female, 9 male; mean age 59.8 years,

age range 37 to 77 years) are presented in Table 1. Duration of disease ranged between 5 months and 23 years (mean 4.85 years). Disease scores – added values for vHIT and bithermal caloric testing for both ears – ranged between 7 and 16 points (mean 11.4 points)(Table 1).

BVP patients did not differ significantly from HCs in trait-anxiety (p=0.41 two-sample ranksum test and p=0.35 two-sample t-test). Similarly, state-anxiety did not differ significantly between HCs and BVP patients; however, it was close to being significantly different (p=0.06 two-sample ranksum test and p=0.06; two-sample t-test).

3.2. MRI

3.2.1. Patients versus healthy controls (HC)

Local gray matter (GM) volume of BVP patients compared to HC was increased in the left retroinsular region / planum temporale, in the left visual cortex area BA17, the left frontal pole, and in the right superior parietal lobule. In the cerebellum, we detected volume increases in crus II of the left hemisphere and the right uvula. Analysis of white matter changes revealed increased local volume in BVP patients in the left planum temporale, reaching into the angular and supramarginal gyri, in areas surrounding the calcarine cortex bilaterally, in the left lateral occipital cortex, and in the central opercular cortex of the right hemisphere. Further, an elongated cluster was located along the anterior cingulate gyrus, bordering the corpus callosum, as well as several clusters in frontopolar regions of both hemispheres (Table 2, Fig. 1).

There were differences in rs-fMRI fluctuation measures between BVP patients and HCs (Fig. 2 top). The detailed list of areas with peak coordinates, center of mass coordinates and cluster sizes can be found in the corresponding supplementary Table 1; here we just list the brain structures which showed changes between groups. Most notable were the differences between groups in the right hippocampus (extending into the right amygdala). Furthermore, we found the cerebellum mostly bilaterally, the brainstem, anterior cingulum, right putamen, PGa (IPL) bilaterally, the posterior insula - with strong right side differences and weak but significant differences on the left -, the areas OP3 and OP4 on the right, the bilateral lateral occipital gyrus overlapping the edge and slightly into the area V5/MT bilaterally, the areas V1 and V2 in the lingual gyrus, the bilateral angular gyrus area hIP1(IPS), the left thalamus, the area PFcm (IPL) bilaterally but most strongly on the right, the anterior insula on the left, area 45 middle frontal gyrus (+inf front gyrus), area Fp1 in the frontal pole, area p32 in the paracingulate gyrus, frontal pole and middle frontal gyrus.

Overlaps between VBM group differences (WM BVP>HC) and rs-fMRI BVP disease duration correlations are depicted in Fig. 3 (middle and bottom). Overlaps in the bilateral frontal pole, precuneus and hippocampal formation are examples of a local concordance of structural (VBM) and functional (rs-fMRI) alterations in BVP patients.

3.2.2. Changes with disease duration

Comparison of local brain volume with disease duration revealed a bilateral decrease of GM volume in the amygdala, in anterior parts of hippocampal and parahippocampal areas, and in the temporal pole. A unilateral GM volume decrease was located in the right thalamus. An increase in GM was observed in the left superior and middle frontal gyri, in an elongated cluster along the right superior occipito-frontal fascicle, and in visual cortex BA17 bilaterally. WM increases were found in the left lateral ventral prefrontal cortex and orbitofrontal cortex, the right caudate, in the left premotor cortex BA6, left lateral occipital cortex and bilaterally in the thalamus, namely in the right anterior nucleus and in the left postero-lateral thalamus / pulvinar. Decreases of white matter correlated with disease duration occurred along the callosal body in the superior corona radiata of both hemispheres (Fig. 4, Fig. 5, Table 2).

There were widespread changes in rs-fMRI fluctuation measures associated with BVP duration (Fig. 2, bottom). The detailed list of areas with peak coordinates, center of mass coordinates and cluster sizes can be found in the corresponding supplementary Table 1. Most notable was the involvement of the left and right hippocampus (right side also protruding into the amygdala). The left hippocampus showed a decrease of amplitude fluctuations with disease duration, while the right hippocampus showed an increase of amplitude fluctuations. There were further areas with positive and negative relations to disease durations.

Overlaps between VBM group differences (WM BVP>HC) and rs-fMRI BVP disease duration correlations are depicted in Fig. 3 (top).

3.2.3. Changes with disease score

A single cluster of volume increase with BVP-score was located in the temporal pole of the right hemisphere. GM decreases in correlation with BVP-score were found in the left frontal operculum, left lateral occipital cortex compatible with V5, and in the right anterior intraparietal sulcus hIP2. We did not find any changes of white matter related to BVP-score (Table 2).

There were widespread changes in rs-fMRI fluctuation measures associated with BVP-score. The detailed list of areas with peak and center of mass coordinates and cluster sizes can be found in the corresponding supplementary Table 1. These areas were the brainstem, the cerebellar hemispheres bilaterally, and the vermis. Further areas were the right putamen, left caudate nucleus, the anterior as well as posterior cingulum, paracingulate gyrus, the anterior insula bilaterally, the left dorsolateral thalamus and right paramedian thalamus, the middle temporal gyrus/ supramarginal gyrus bilaterally (outside of V5/MT, close to or in the areas PGa(IPL)), the bilateral LOC (lateral occipital cortex), the right precentral gyrus, the SMA (supplemental motor area), area 3a (postcentral gyrus/anterior supramarginal gyrus), right OP3/OP2, and left superior temporal gyrus (STG) extending into the left posterior insula as a subcluster. In the frontal cortex clusters in the frontal pole, the superior frontal gyrus and the middle frontal gyrus bilaterally were seen.

3.2.4. Changes with trait anxiety

Correlations of GM volume increases with Trait Anxiety values, calculated for both groups counted together, were seen in the thalamus bilaterally, in the right posterior granular insula Ig2, in the left planum temporale, and bilaterally in a cingular region compatible with area CSv (Fig. 6, red/yellow). Further clusters were detected in the right superior frontal gyrus, the right orbito-frontal cortex, and a cluster in the right precuneus that overlapped with parts of the optic radiation. GM volume decreases associated with Trait Anxiety values were disclosed in right lateral occipital cortex only, compatible with area V5.

White matter volume increases with Trait Anxiety were detected bilaterally in the inferior longitudinal fasciculus adjacent to Heschl's gyrus, in the left temporo-occipital fusiform cortex, the left supramarginal gyrus, in the bilateral premotor cortex near the GM changes in putative area CSv, and in the left lateral and lateral ventral prefrontal cortex. Further clusters were found stretching from the precentral gyrus into the corticospinal tracts of both hemispheres (Fig. 6, green), and in the right hemisphere into short cingulate fibers. No areas with WM volume decreases were observed in relation to Trait Anxiety.

3.2.5. Patterns of rs-fMRI fluctuation measures

All significant clusters, detected in the analysis of rs-fMRI fluctuation measures data, were directionally correlated without any mixed results. This means that either all measures were positive or negative. In the supplemental materials selected clusters and their contrast estimates for the different fluctuation measures were shown (suppl. Fig. 2).

4. Discussion

In this multimodal imaging study, it was investigated how the reduced or absent bilateral peripheral vestibular input, that BVP patients experience, is substituted and compensated for in multisensory and sensorimotor processing. Structural alterations were found in various distinct areas which can be assigned to different functional

Table 2
Results of VBM for gray and white matter.

Grey matter volumetry Site	size	peak (x y z)	peak t-value	White matter volumetry site	size	peak (x y z)	peak t-value
BVP duration positive				*BVP duration positive*			
superior occipito-frontal fascicle	649	21 13 22	7.50	frontal pole / ContB_PFClv_1	385	-35 53 -13	6.92
superior occipito-frontal fascicle		21 23 14	6.19	frontal pole / SalVentAttnB_OFC_1		-27 46 -14	4.30
callosal body		18 3 27	5.18	caudate	316	13 7 14	6.11
visual cortex V1 BA17	474	-17 -86 8	7.17	lat. occipital cortex, inferior division	125	-40 -87 3	4.98
optic radiation	109	20 -73 16	5.53	premotor cortex BA6	424	-19 -9 65	4.73
superior frontal gyrus	227	-11 27 50	5.40	premotor cortex BA6		-10 -5 70	4.54
middle frontal gyrus / ContA_PFCl_3, DefaultB_PFCl_1	424	-48 13 34	4.80	thalamus / ant. nucleus	464	11 -11 6	4.39
visual cortex V1 BA17	316	20 -86 4	4.56	thalamus / pulvinar	834	-15 -24 13	4.36
visual cortex V1 BA17		15 -95 2	4.08	thalamus / lateral posterior nucleus		-19 -16 13	4.36
BVP duration negative				*BVP duration negative*			
amygdala, laterobasal group	3247	-33 -1 -29	5.01	callosal body / sup. corona radiata	265	-20 -11 33	4.25
hippocampus subiculum		-23 -12 -30	4.64	callosal body / sup. corona radiata		-19 1 32	3.60
temporal pole		-39 13 -46	4.60	callosal body / sup. corona radiata	397	21 -6 35	4.13
hippocampal-amygdaloid transition area	1465	21 -11 -8	4.79	callosal body / sup. corona radiata		21 -17 33	3.95
amygdala		25 -4 -16	4.19	callosal body / ant. corona radiata	392	21 25 20	4.11
amygdala, centromedial/superficial group	1998	-18 -7 -8	4.78	callosal body / sup. corona radiata		20 11 28	3.77
optic radiation		-30 -19 -10	4.71				
temporal pole		-20 5 -27	4.27				
temporal pole	510	53 6 -29	4.30				
temporal pole		63 3 -30	3.78				
cerebellum / dentate	136	-12 -50 -25	4.19				
parahippocampal gyrus, ant. division	229	21 -10 -37	4.08				
thalamus	144	14 -23 18	4.02				
cerebellum I-IV	121	5 -47 -10	3.63				
BVP score positive				*BVP score positive*			
temporal pole	300	52 8 -30	3.85		no clusters		
temporal pole		62 3 -31	2.80				
BVP score negative				*BVP score negative*			
frontal operculum	111	-46 14 -6	4.57		no clusters		
lateral occipital cortex	620	-56 -70 14	4.31				
lateral occipital cortex / V5		-47 -76 6	3.95				
anterior intra-parietal sulcus hIP2	186	43 -44 51	4.13				
Trait Anxiety positive				*Trait Anxiety positive*			
superior frontal gyrus / premotor cortex BA6	2192	17 -3 64	7.93	temporal occipital fusiform cortex	865	-38 -56 -11	5.77
superior frontal gyrus / premotor cortex BA6		14 9 62	4.50	temporal occipital fusiform cortex		-40 -65 -9	3.75
superior frontal gyrus / premotor cortex BA6		15 6 70	4.21	inferior parietal lobule PFop	1169	-54 -31 27	5.73
thalamus / fornix	2096	11 -24 19	6.65	inferior parietal lobule / supramarginal gyrus		-62 -32 28	5.01
optic radiation / precuneous	765	-20 -77 19	5.53	premotor cortex BA6	541	7 1 62	5.33
optic radiation / precuneous		-22 -65 27	4.43	middle frontal gyrus / ContA_PFCl_3	508	-35 10 36	5.23
planum temporale	334	-56 -24 10	5.03	frontopolar cortex / ContA_PFClv_1,	180	-41 37 11	4.73
insula Ig2 / heschl's gyrus	1260	42 -17 9	4.89	ContA_PFClv_2, SalVentAttnB_PFCl_1			
insula Ig2		35 -25 3	3.78	premotor cortex BA6	3412	-3 -11 52	4.62
thalamus / fornix	679	-10 -27 18	4.82	corticospinal tract / precentral gyrus		-29 -11 50	0.21
thalamus		-9 -8 19	3.89	corticospinal tract / callosal body		-21 -11 34	3.97
frontal orbital cortex / DefaultB_PFCv_1	378	38 19 -18	4.45	callosal body	283	13 1 41	4.60
cingulate gyrus, post. division / CSv	239	-15 -20 46	3.91	superior frontal gyrus / ContA_PFCd_1	3061	22 2 59	4.41
cingulate gyrus, post. division / CSv		-14 -26 37	3.88	corticospinal tract / precentral gyrus		15 -17 47	4.31
cingulate gyrus, post. division / CSv	200	17 -32 42	3.81	corticospinal tract / precentral gyrus		9 -22 60	3.99
				inferior longitudinal fasciculus	192	44 -27 1	3.93
				precentral gyrus	106	-4 -26 56	3.86
				inferior longitudinal fasciculus	229	-46 -28 -3	3.84
Trait Anxiety negative				*Trait Anxiety negative*			
lateral occipital cortex / V5	147	61 -63 3	4.06		no clusters		
patients versus controls				*patients versus controls*			
planum temporale	2296	-39 -36 15	5.95	parahippocampal gyrus, anterior division	656	-24 1 -33	5.81
cerebellum crus II	946	-48 -60 -47	5.19	frontal pole / SalVentAttnB_PFCl_2	193	25 49 27	5.80
cerebellum crus II		-37 -73 -46	4.16	frontal pole / SalVentAttnB_PFCl_2		20 55 22	3.85
visual cortex V1 BA17	160	-4 -93 6	5.16	intracalcarine cortex	1291	-12 -68 8	5.64
frontal pole / ContB_PFClv_2	313	-32 63 -2	4.63	visual cortex V1 BA17 / precuneous cortex		-13 -56 5	5.52
superior parietal lobule 5L	257	13 -50 61	4.41	lingual gyrus		-13 -60 -2	4.49
cerebellum crus II / uvula	567	12 -82 -35	4.28	frontal pole / ContB_PFClv_2	1306	-26 50 -1	5.30
				frontal pole / SalVentAttnB_PFCl_1		-34 44 4	3.94
				frontal pole		-35 47 -8	3.93

(*continued on next page*)

Table 2 (*continued*)

Grey matter volumetry Site	size	peak (x y z)	peak t-value	White matter volumetry site	size	peak (x y z)	peak t-value
				frontal orbital cortex / DefaultB_PFCv_2	672	47 33 -14	5.23
				cingulate gyrus, ant. division	1219	-4 37 7	5.21
				cingulate gyrus, ant. division		-1 23 24	4.06
				frontal pole / LimbicB_OFC_3	1243	-10 43 -26	5.13
				central opercular cortex / operculum OP4	244	61 -7 10	4.94
				frontal orbital cortex / ContA_OFC_1	305	-39 37 -7	4.76
				planum temporale	936	-42 -40 18	4.73
				angular gyrus / supramarginal gyrus		-43 -51 21	4.03
				angular gyrus / supramarginal gyrus		-49 -49 16	3.92
				lateral occipital cortex	295	-33 -88 5	4.67
				frontal pole / LimbicB_OFC_3	474	-14 59 -17	4.64
				visual cortex V1 BA17	475	18 -56 9	4.27
				visual cortex V1 BA17 / intracalcarine cortex		4 -66 7	4.10
				visual cortex V1 BA17 / precuneous cortex		10 -53 9	4.04
				lateral occipital cortex	117	-38 -85 17	4.20
				central opercular cortex	228	44 -2 12	4.14
				middle frontal gyrus / SalVentAttnB_PFCl_2	129	-27 36 26	4.02
				medial frontal cortex / LimbicB_OFC_3	120	7 44 -25	3.89
				callosal body / cingulate cortex	106	-5 -11 32	3.77
controls versus patients				*controls versus patients*			
lateral occipital cortex	320	-46 -84 10	4.53		no clusters		

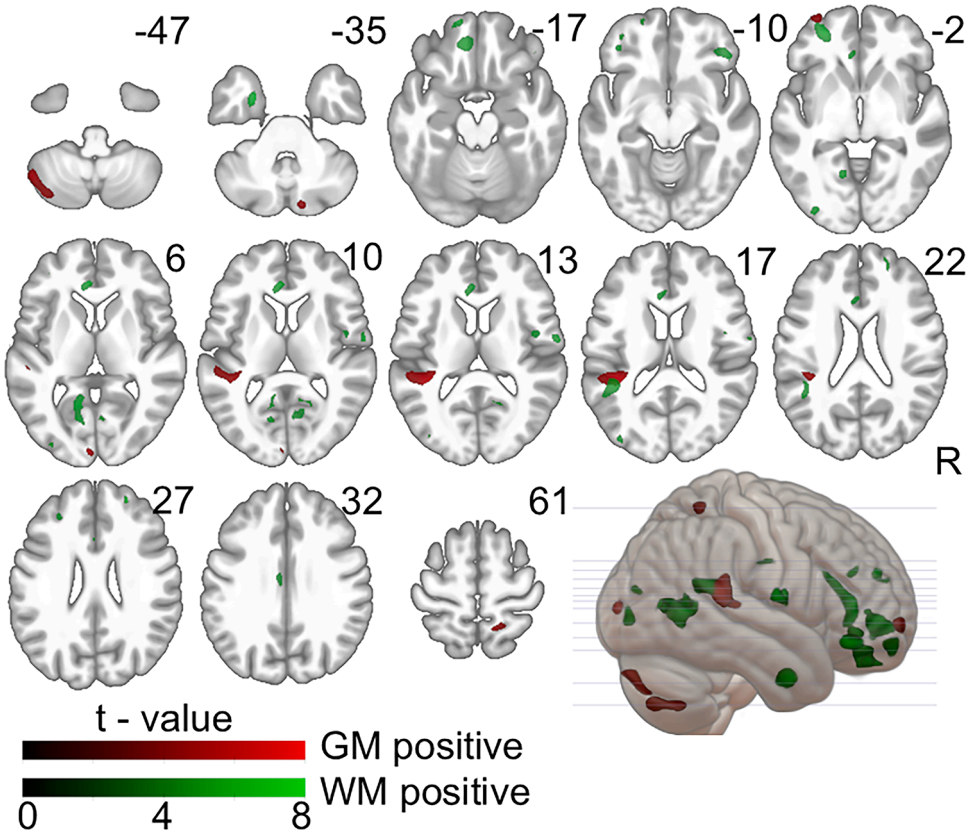

Fig. 1. *VBM results for BVP patients compared to healthy controls* (HC), projected onto a mean T1 image of all subjects in MNI space. Increases of local gray matter volumes are depicted in red, increases of local white matter volumes in green. Numbers represent positions of axial slices in mm above the anterior commissure. In addition, slice positions are depicted on the glass brain view (two sample t-test, n = 15/15, $p<0.001$ unc., $k\geq100$).

systems. Gray and white matter changes in local combination with rs-fMRI changes were seen in:

- multisensory vestibular cortex areas with the core region of the left posterior insula/retroinsular area and the neighboring planum temporale, angular and supramarginal gyri, and left premotor cortex BA6, as well as in the right temporal pole,

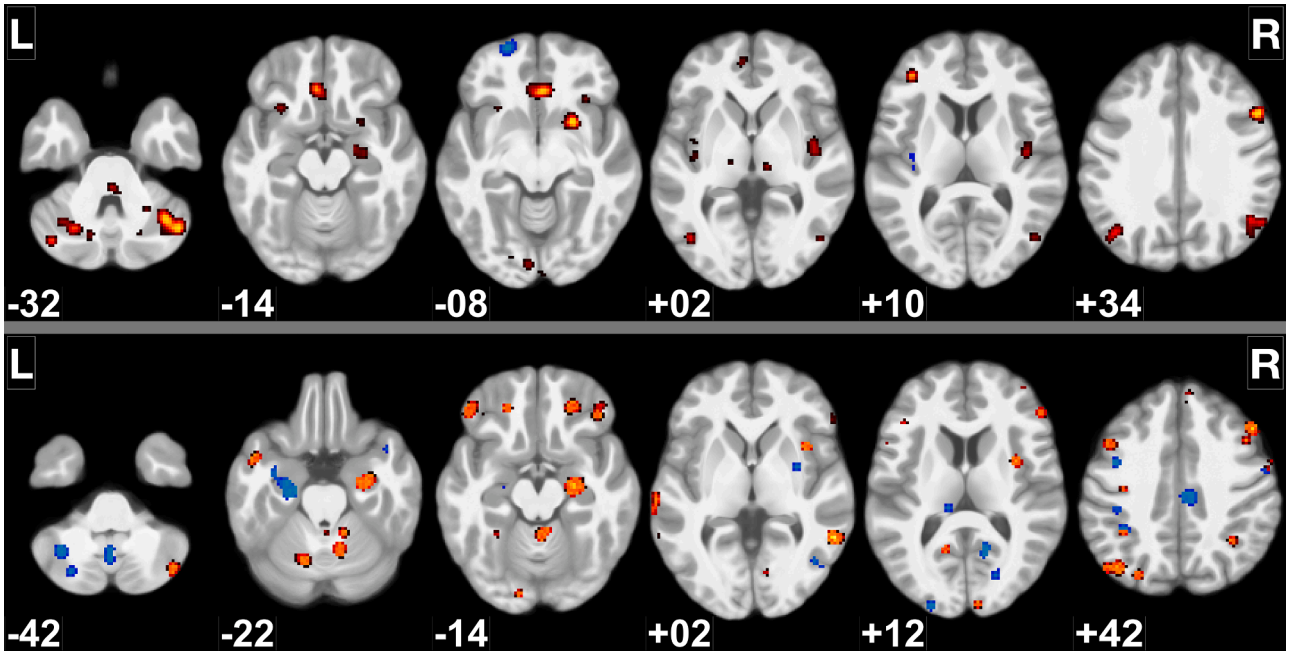

Fig. 2. *Group differences and correlation with disease duration in resting-state amplitude fluctuations.* Top: Significant amplitude fluctuation changes on axial slices for BVP-vs-HC, with red-yellow color map indicating where BVP patients had higher fluctuations than HCs. Bottom: Significant correlations between amplitude fluctuations and BVP disease duration. Red-yellow color map indicating where increasing BVP disease duration led to increasing amplitude fluctuations and blue-green color map indicating where increasing BVP disease duration led to decreasing amplitude fluctuations.

- bilateral anterior hippocampal formation and adjacent amygdala,
- bilateral visual cortex including V1 and V5,
- bilateral thalamus,
- bilateral prefrontal cortex including PFCl, PFClv, PFCv, PFCd, OFC,
- bilateral cerebellar hemispheres and uvula,
- bilateral pyramidal tract.

Volume increases and decreases appeared either unilaterally or bilaterally, depending on the different methods of data analysis and the various correlations with other factors largely overlapping with changes in functional connectivity (rs-fMRI)(Fig. 3). Correlating the brain volumes with the disease duration in BVP revealed a gray matter atrophy in the anterior divisions of the hippocampus/ parahippocampal formation bilaterally as well as in the bilateral amygdala. On the other hand, gray matter *increases* were seen in the bilateral visual cortex (BA 17) and the left frontal pole; white matter increases were seen in the left dorsolateral thalamus, left frontal pole, right anterior thalamus and right caudate nucleus. This pattern of increases and decreases distributed throughout the entire brain reflects the known interaction between the sensory and motor systems. A recent study on altered functional connectivity in patients with chronic unilateral – rather than bilateral - vestibulopathy revealed a similar pattern of areas involved when seed-based functional connectivity and voxel-mirrored homotopic connectivity analyses were applied (Xing et al., 2024).

So far studies of voxel-based morphometry analyses in BVP had focused on the hippocampal complex after a hippocampal atrophy had been disclosed in complete bilateral vestibular loss (Brandt et al. 2005). This was later examined in incomplete BVP (Kremmyda et al., 2016; Göttlich et al., 2016; Smith, 2017; rat: Smith et al., 2005) with inconsistent results. In summary, it was shown that bilateral vestibular loss led to a hippocampal atrophy, the extent of which depended on the degree of vestibular failure, and some studies even did not find any differences compared to healthy controls (human: Cutfield et al., 2014; Dordevic et al., 2021; rat: Zheng et al., 2012). The only multimodal imaging study on whole brain analysis also described, with respect to brain morphology, a decreased gray matter volume in the bilateral posterior parahippocampal gyri. Beyond that, volume decreases were described in the right precentral gyrus, anterior cingulate gyrus, right middle temporal gyrus, as well as gray matter volume increases in the right superior frontal gyrus (Lee et al., 2023). The correlation analysis with a "vestibular disorders activity of daily living" scale showed a bilateral decrease in the calcarine gyri. However, its functional significance was not explicitly discussed.

In the current study, the patterns of volume and connectivity changes exhibited a certain degree of local overlap but appeared more complex and differentiated. They should be viewed from a systemic perspective that takes into account the multifunctional roles of the vestibular system for motion perception, spatial orientation, balance control, cognition and emotion. From tracer studies in rat it is known that adaptive neuroplasticity after bilateral vestibular loss is not a uniform process but is composed of complex spatial and temporal patterns of structure-function coupling in networks for vestibular, multisensory, and motor control (Antons et al., 2022). In the following the individual localizations of current structural and functional alterations in BVP patients and their presumed significance will be discussed in interaction or interplay with the other sensory, motor, cognitive, and emotional networks.

4.1. *Vestibular cortical network*

The posterior insula, retroinsular and opercular region (Grüsser et al., 1990 a,b; Guldin and Grüsser, 1998; Brandt et al., 1994) are recognized as the core region of the vestibular cortical network – called the parieto-insular vestibular cortex (PIVC) in monkeys (Grüsser et al., 1990 a,b; Guldin and Grüsser, 1998). The cortical vestibular system is determined by a thalamo-cortical hemispheric lateralization (Dieterich et al., 2017). This was first shown in a PET study during caloric vestibular stimulation with a right-hemispheric dominance in right-handers and a left-hemispheric dominance in left-handers (Dieterich et al., 2003). The hemispheric dominance was confirmed by fMRI during galvanic vestibular stimulation and auditory-evoked vestibular (otolith) stimulation (Fink et al., 2003; Schlindwein et al., 2008; Janzen et al., 2008) as well as in three MRI meta-analyses (zu Eulenburg et al., 2012; Lopez et al., 2012; Neumann et al., 2023). The lateralized right-sided upper brainstem-thalamic function is part of the

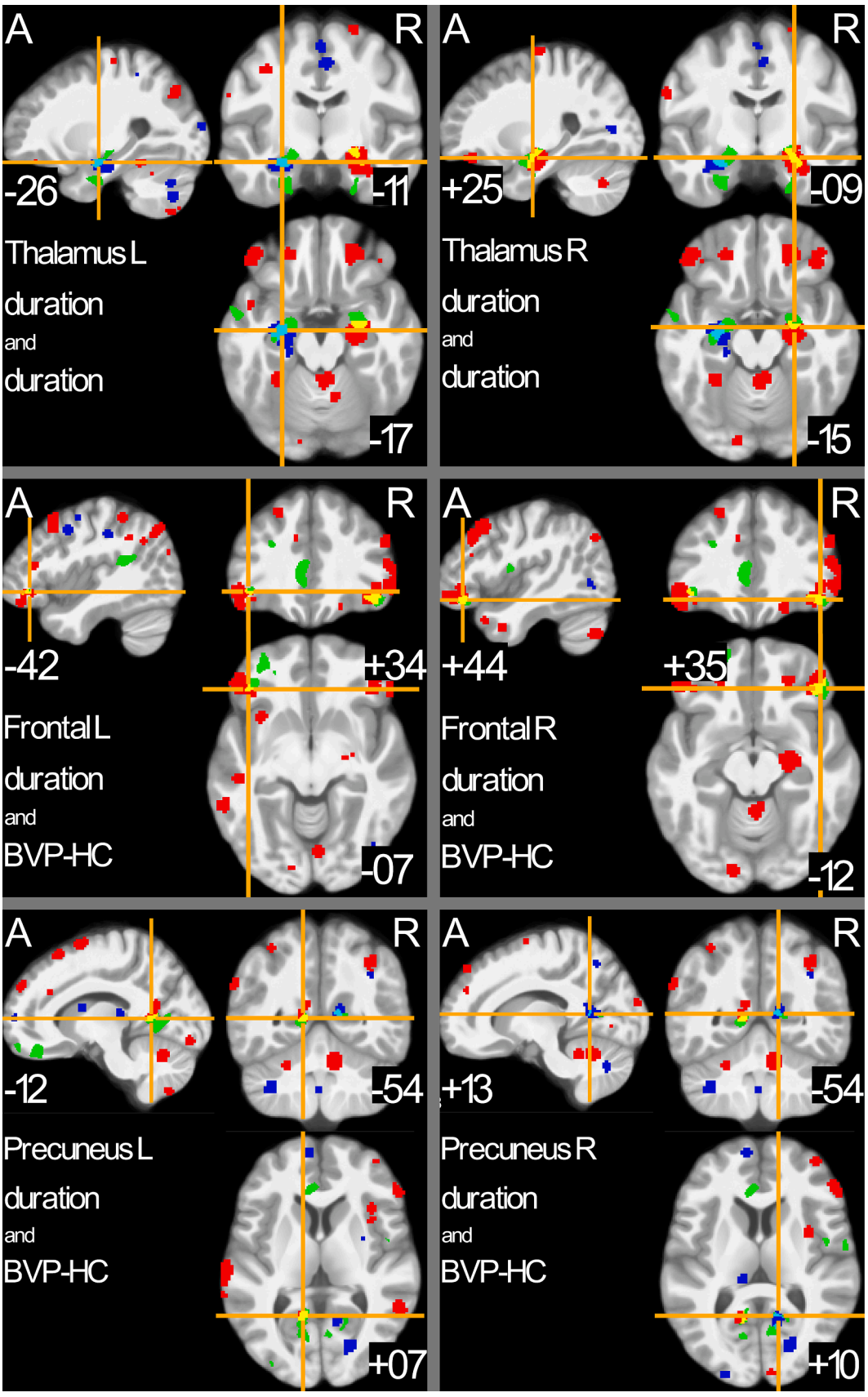

(caption on next page)

Fig. 3. *Overlaps between VBM analysis and resting-state analyses (rs-fMRI).* Top: overlap of rs-fMRI correlations with BVP disease duration and VBM correlations with disease duration, focused on the overlap of left and right hippocampus. Middle and bottom: overlap of rs-fMRI correlations of BVP disease duration and VBM group differences between BVP patients and HCs, focused on frontal regions (middle) and precuneus (bottom). An orange crosshair marks the overlap of interest in each panel. Red: increases in rs-fMRI amplitude fluctuations with longer disease duration. Blue: decreases in rs-fMRI amplitude fluctuations with longer disease duration. Green: VBM decreases with disease duration (top) or VBM decreases in the patients vs. HCs (middle, bottom). Yellow: overlap between rs-fMRI increases and VBM decreases. Cyan: overlap between rs-fMRI decreases and VBM decreases. In the top row left, the left hippocampus shows a volume decrease overlapping a decrease in rs-fMRI amplitude fluctuations (cyan). In the top row right, the right hippocampus shows a volume decrease overlapping an increase in rs-fMRI fluctuations (yellow). The middle row gives yellow overlaps of rs-fMRI fluctuation increases with VBM volume decreases in frontal cortex areas (fronto-orbital and ventral prefrontal cortex). The bottom row depicts overlaps between rs-fMRI fluctuations and VBM volume decreases: the left precuneus shows increases of rs-fMRI fluctuations, whereas the right precuneus shows decreases of rs-fMRI fluctuations.

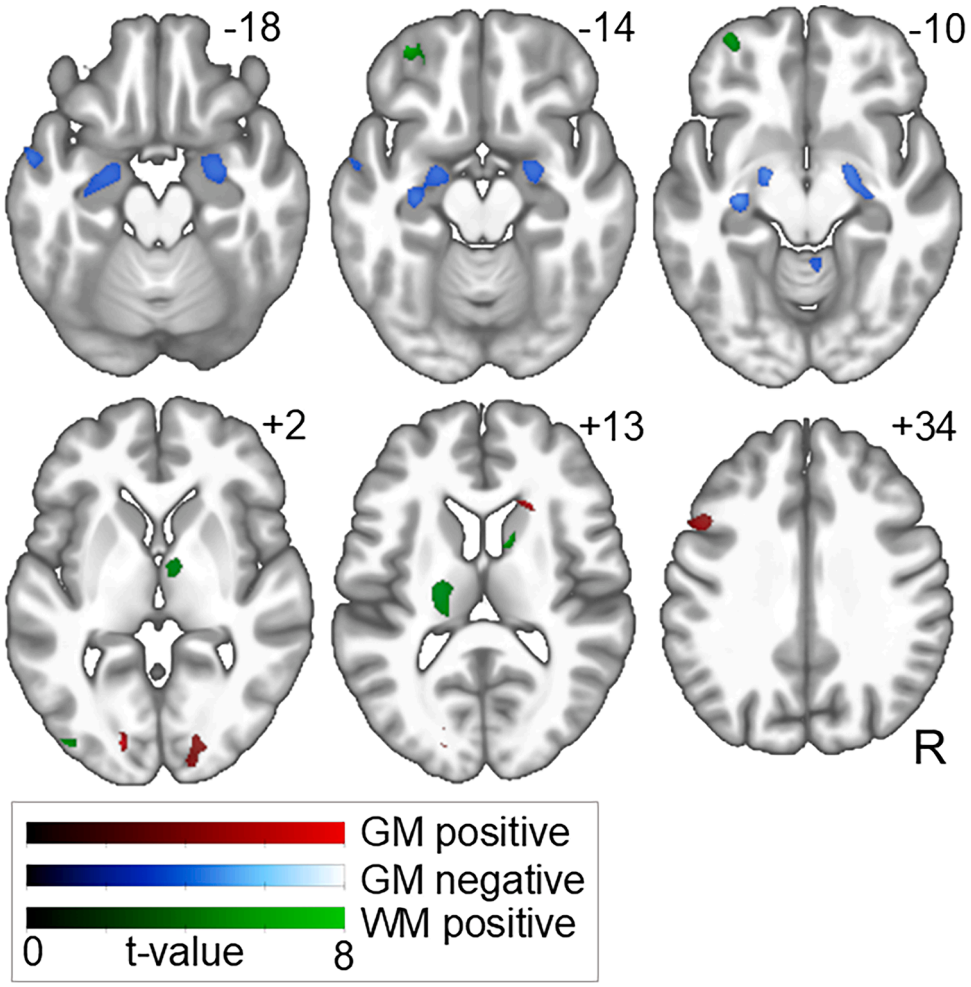

Fig. 4. *Disease Duration (VBM).* Brain volume differences associated with disease duration obtained from BVP patients and matched healthy controls (one sample t-test with covariates, n=29, $p<0.001$ unc., $k\geq100$). Increases and decreases in gray matter (GM) are rendered in red and blue, respectively. Increases in white matter (WM) are depicted in green. VBM results are overlaid onto a mean image of the group of subjects, numbers provide the slice position in mm above the anterior commissure.

dominant right-sided cortical and subcortical vestibular system (Dieterich et al., 2017).

Instead of the anticipated atrophy in the right insular area in BVP, the current study actually showed an increase in the volume of the left posterior/retroinsular area and the nearby parieto-opercular region (Fig. 1). Interestingly, in the right insula neither atrophy nor an increase was found, suggesting that it continues to function possibly with reduced vestibular input and additionally input from other sensory systems to compensate for the lacking vestibular information. The increase in the volume of the left insula suggests that it may have assumed a more prominent role in motion perception and spatial orientation by interacting more strongly with other networks. We are not aware of other studies on insular volume changes in BVP. Amplitude fluctuations in another part of the posterior insula bilaterally disclosed changes between groups (Fig. 2, top). The right posterior insula showed greater amplitude fluctuations for BVPs than the left. Thus, although we did not detect local volume changes in the right posterior insula, functional alterations were found in the form of increased amplitude fluctuations.

In terms of vestibular cortical network structures, the vestibular core region in the posterior insula was shown to receive input from the prefrontal cortex (DLPFC) that modulates vestibular signals (McCarthy et al., 2023, 2025). This modulation, a suppression of the vestibular sensations elicited by electrical vestibular stimulation over the mastoids, was initiated by simultaneous transcranial sinusoidal electrical stimulations of the DLPFC. Thus, the authors formulated the hypothesis of a top-down regulation of vestibular inputs (McCarthy et al., 2023).

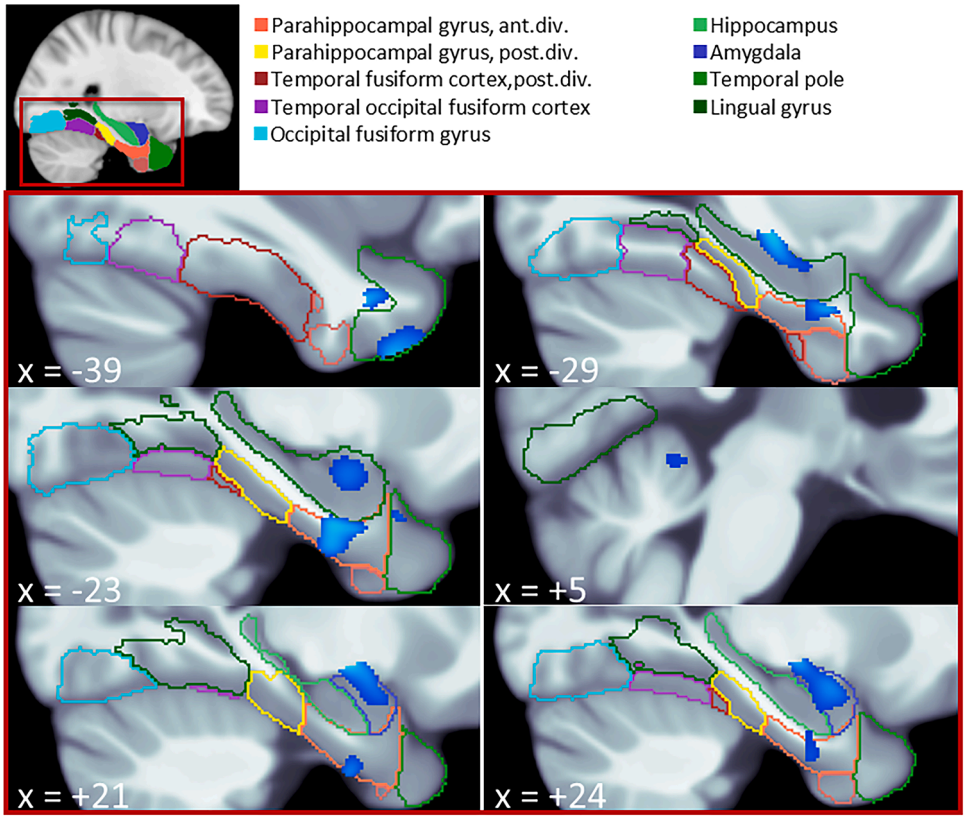

Fig. 5. *Disease Duration and hippocampal VBM.* Enlarged illustration of gray matter decreases associated with disease duration in hippocampal, parahippocampal and amygdala regions. Borders of anatomical structures are extracted from the Harvard-Oxford cortical and subcortical structural atlases and rendered onto sagittal slices through a group mean image. MNI coordinates provide the distance from the anterior commissure (one sample t-test with covariates, n=29, p<0.001 unc., k≥100).

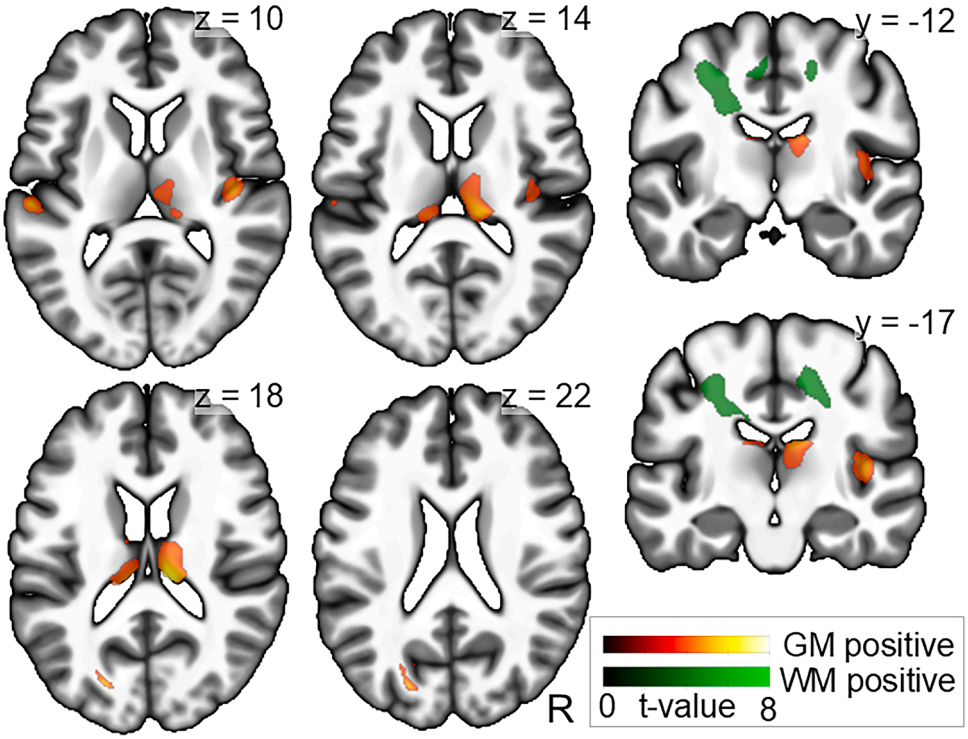

Fig. 6. *VBM increases with trait anxiety.* Local increases in gray matter (red/yellow) and white matter (green) volume associated with trait anxiety values for all participants. VBM results were rendered onto a group mean image, labels give slice locations in MNI coordinates (one sample t-test with covariates, n=29, p<0.001 unc., k≥100).

4.2. Hippocampal formation and amygdala

In BVP patients with complete vestibular loss (Brandt et al., 2005), a *bilateral hippocampal* atrophy had been disclosed that was related to the deficit in spatial memory and navigation (Morris-Water task). This was confirmed in the current study on patients with incomplete BVP dependent on the duration of the condition (Figs. 4, 5). There are earlier animal studies on vestibular-hippocampal interactions which had already hypothesized that the hippocampus may be important for compensation of vestibular function following a peripheral loss of input (Smith, 1997; Smith et al., 2005). The exact localization of the volume reduction within the hippocampal formation related to disease duration in the present study was located in the anterior part of the hippocampus bilaterally including the anterior division of the parahippocampal gyrus and the bilateral amygdala (Fig. 5). This hippocampal atrophy in the anterior regions of our BVP patients serves as structural evidence supporting an earlier hypothesis that was formed by reviewing anatomical, electrophysiological, and imaging data (Hüfner et al., 2011a). The latter had suggested that vestibular input is primarily processed in the anterior part of the hippocampal formation, whereas visual cues are primarily integrated in the posterior part (Hüfner et al., 2011a). This current confirmation supports the view of a spatial separation of visual and vestibular processing in the hippocampal formation with a twofold functional consequence for substitution of missing input from either system or a task dependent shift of the sensorial weight to the more reliable modality (Hüfner et al., 2011a). In contrast, Lee and coworkers described volume reductions in the posterior rather than the anterior hippocampus without referring to whether the processing of visual or vestibular input is involved (Lee et al., 2023). Although the hippocampus is not typically considered part of the visual system, it is involved in certain aspects of vision such as spatiotemporal similarity via the ventral visual stream (Turk-Browne, 2019). Functional and structural separation and plasticity of the hippocampus has also been shown in individuals with extensive balance training (professional dancers and slackliners) exhibiting smaller anterior hippocampal formation volume with larger volumes in the posterior hippocampal formation indicating an increased utilization of visual cues for their balance performance (Hüfner et al., 2011b).

The novel finding of an associated bilateral atrophy of the *amygdala* (Fig. 5) can be best explained by the functional interaction of the overlapping fMRI activation patterns of the anxiety-emotional and the vestibular-sensory networks, as described in a recent meta-analysis (Neumann et al., 2023). This was further assessed in a vestibular stimulation and fear conditioning paradigm in a group of individuals who underwent both types of stimulation subsequently (Lotze et al., 2025). Thus, the amygdala atrophy is the result of the plastic reorganization due to the emotional consequences of the loss of vestibular input. With respect to the neural level, fear conditioning is thought to primarily involve a network including the medial prefrontal cortex (PFC), amygdala and hippocampus (Quirk and Mueller, 2008; Brown et al., 2025). From a series of detailed rodent experiments, a map of the fear/anxiety circuit is known in which the amygdala and hippocampus store fear memories, while the medial PFC integrates information about the conditioned stimulus modulated by contextual information from the hippocampus (Quirk and Mueller, 2008). In parallel, human imaging studies found a coupling between the amygdala, ventromedial PFC and hippocampus during both fear expression and fear extinction (Brown et al., 2025; Milad and Quirk, 2012; Kalisch et al., 2006).

4.3. Visual cortex

The current study showed significant volume increases in the bilateral visual cortex, V1 and V5 in BVP patients (Fig. 1). This is in line with the previously reported reciprocal decrease in volume in the anterior vestibular hippocampus and the increase in the visual part of the hippocampus in professional dancers (Hüfner et al., 2011b). These bilateral volume increases and amplitude fluctuation changes within the visual cortex correlated to the duration of the disease (Figs. 2, 4), corresponding to a visual substitution of the missing vestibular input (Bense et al., 2004; Dieterich et al., 2007). Gray matter volume increases of the visual cortex also correlated with the level of Trait Anxiety (Fig. 6). This supports a probable aid by visual cues to stabilize balance and overall well-being in BVP patients with increased Trait Anxiety.

4.4. Thalamus

The significant volume increases in the left dorsolateral and right anterior *thalamus* (Fig. 4), depending on the duration of vestibular loss, align with integrative multisensory functions that include visual, vestibular, proprioceptive, and somatosensory stimuli beyond a simple sensory relay station (Wijesinghe et al., 2015). The same is true for the increased amplitude fluctuations of the right paramedian and left posterolateral thalamus (Fig. 2). Thalamic subnuclei do not serve only as provincial hubs but also in higher order nuclei as connector hubs (Hwang et al., 2017; Brandt and Dieterich, 2019). A graph-theoretic analysis of thalamocortical functional connectivity data revealed that thalamic subdivisions display network properties that are capable of integrating multimodal information across diverse cortical functional networks (Hwang et al., 2017).

4.5. Frontal cortex and pyramidal tract

The prefrontal cortex (PFC) influences subcortical structures such as the thalamus and the vestibular system via complex neural networks. Here, the bilateral white matter volume increases as well as amplitude fluctuation changes in the lateral, lateral ventral, and ventral prefrontal and orbitofrontal cortex (Figs. 1, 2; Table 2, Supplementary Table 1) can best be explained by an activated top-down regulation of postural balance, especially in increased Trait Anxiety, for a consciously enhanced control of stance and gait via the pyramidal tract which was also significantly increased in volume bilaterally (Fig. 6). It is known that the dorsolateral PFC can be influenced by the brain's anxiety and fear system through its connections with the amygdala (Brown et al., 2025; Milad and Quirk, 2012; Kalisch et al., 2006). Additionally, both the dorsolateral and ventrolateral PFC were involved in emotional/anxiety as well as vestibular processing (Neumann et al., 2023; Lotze et al., 2025), and they also modulate the vestibular cortex in the posterior insula (McCarthy et al., 2023). A suppression of the vestibular sensations in healthy subjects was found, elicited by electrical (galvanic) vestibular stimulation of the mastoids and simultaneous transcranial sinusoidal electrical stimulations of the DLPFC (McCarthy et al., 2023). Thus, the vestibular core region in the posterior insula received input from the DLPFC, and a top-down control of vestibular inputs was hypothesized (McCarthy et al., 2023).

In summary, this means since the PFC plays a crucial role in integrating and modulating information from the vestibular system, which is responsible for balance, it helps to link sensory signals with cognitive processes to adjust posture and movements. This corresponds to our current data in BVP patients with postural imbalance in whom the PFC is increasingly involved in the modulation of unstable and altered inputs (i.e., reduced and unstable vestibular information and substitution by visual input). Thus, the PFC contributes to the conscious perception of balance changes and the coordination of movements. It acts as a bridge between sensory signals and higher cognitive processing including anxiety and fear processing.

The *pyramidal tract* primarily controls voluntary skeletal muscle movements, especially fine and precise movements, modulated by other motor (e.g., precentral gyrus and extrapyramidal system) and sensory systems to enable coordinated actions. This is particularly important for BVP patients as they need a more conscious control of posture and gait to compensate for the vestibular deficiencies. For that it is helpful that the PFC integrates signals from various sources, including motor pathways,

to ensure comprehensive movement control and adaptation to balance changes. These functional aspects align with the widespread white matter volume increases we observed with Trait Anxiety, extending from the precentral gyrus into the corticospinal tracts of both hemispheres (Fig. 6, green).

4.6. Cerebellum

In the cerebellum, the volume increases in crus II of the left hemisphere and the right uvula can be explained by an enhancement of a second motor cortical–cerebellar loop (Kelly and Strick, 2003) that shows a convergent representation of movement and sensory information from the whole body. This is related to the imbalance and thus enhanced conscious postural control in BVP patients and corresponds to the increased connectivity in both cerebellar hemispheres in order to compare the mismatch between expected and actual activity within the cerebellar circuitry. Amplitude fluctuations in the bilateral cerebellar hemispheres and the vermis disclosed changes between groups and correlation with disease duration and BVP score. The left cerebellar hemisphere and the vermis showed a negative correlation with disease duration, while the right cerebellar hemisphere had a positive correlation (Fig. 2). The decrease in amplitude fluctuations in the left cerebellum and vermis, and the associated increase in amplitude fluctuations in the opposite supratentorial hemisphere (including the motor and vestibular systems) is well in line with the reciprocal connectivity of the sensorimotor system. In combination with a crosswise organized cerebellum, upregulation of one leads to downregulation of the other. It is known that nerve fibers of the cerebellum and neocortex cross differently with motor areas in the left cortex and right cerebellum guiding right motor function. This interpretation is supported by the fact that the predominant output of the cerebellum through the Purkinje cells is mainly inhibitory (Jelitai et al., 2016; Judd et al., 2021).

Furthermore, the cerebellum is also embedded in fear and emotional processing, which has been shown in both conditioned and unconditioned responses to threating stimuli in addition to encoding and storage of fear memory (Couto-Ovejero et al., 2023). In line with this, a posterior cerebellar contribution had been described for fear conditioning (Medina et al., 2002; Couto-Ovejero et al., 2023).

4.7. Limitations

Limitations in the interpretation of the data stem from the small sample size and heterogeneity of the BVP patients regarding the residual vestibular function in the right and left inner ear, as well as the individual duration of the disease. Another limitation may be the age of the patients with BVP, in so far as they are often elderly (mean age 59.8 years), which we attempted to balance out by selecting age-matched healthy controls. The relatively small number of enrolled BVP patients was due to factors like their older age, the requirement that they had absolutely no cognitive deficits, their willingness to actually undergo an MRI, and the absence of any MRI contraindications like having a pacemaker.

A further limitation might be the influence of magnetic vestibular stimulation (MVS) which occurs due to the main magnetic field of the MRI (Roberts et al., 2011) and was shown to influence rs-fMRI networks (Boegle et al., 2016, 2017, 2020). MVS was shown to influence healthy controls but was absent for patients with complete bilateral vestibular loss (Roberts et al., 2011). Therefore, MVS might have added noise to the rs-fMRI signal, and more so for the healthy controls, less in the BVP patients depending on the extent of their peripheral vestibular loss, i.e., greater loss leading to less MVS derived noise in rs-fMRI of BVP patients. Given that we mainly found group differences to be larger for BVP patients, this additional noise in HC seems to have had little influence on rs-fMRI amplitude fluctuation measures. Furthermore, given that we found changes related to disease duration, which is not related to disease score and hence not strongly related to MVS influence, we suggest that MVS was of little influence.

5. Conclusion

The methodological combination of structural (VBM) and functional (rs-fMRI) imaging including various correlation analyses revealed that a bilateral reduction of peripheral vestibular input affects multiple networks from the cerebellum up to the cortical hemispheres. A major intention was to determine specific alterations involved in the compensation or substitution of deficits in one sensory system by other networks for perceptual, sensorimotor balance control, cognitive and emotional functions. Taking into account the findings of earlier animal and human studies allowed some interpretations of the current data. Three examples illustrate the cross-system structural and functional integration: 1. The atrophy of the anterior hippocampal/ parahippocampal formation aligns with the previously described impairments in spatial memory and navigation. 2. The overlap of the networks for vestibular function and emotion such as anxiety correspond to other studies that indicate the involvement of the cerebellum, the amygdala, and the prefrontal cortex within a broadly distributed emotional system. 3. The anxious processing of the balance disorder, caused by the loss of vestibular information, apparently activates the cognitive conscious control in a top-down mode from the prefrontal cortex via the pyramidal tract involving reciprocal cerebellar structures organized in a crossed-hemispheric manner.

Funding

RB was funded by the German Foundation for Neurology (DSN, projects 80766090 and 80721019). MD was supported by the DSN (projects 80721017 and 80766090) and the Deutsche Forschungsgemeinschaft (DFG, German Research Foundation) under Germany's Excellence Strategy (Munich Cluster for Systems Neurology: EXC 2145 SyNergy).

CRediT authorship contribution statement

Marianne Dieterich: Writing – original draft, Visualization, Investigation, Funding acquisition, Data curation, Conceptualization. **Thomas Stephan:** Writing – review & editing, Methodology, Formal analysis, Data curation. **Lena Fabritius:** Data curation. **Rainer Boegle:** Writing – original draft, Methodology, Investigation, Formal analysis, Data curation. **Thomas Brandt:** Writing – review & editing, Supervision, Data curation, Conceptualization.

Declaration of competing interest

The authors have nothing to declare.

Acknowledgements

Thanks to Sandra Becker-Bense for supporting MD in selecting the patients in the study. We are grateful to Katie Göttlinger for copy editing the manuscript.

Supplementary materials

Supplementary material associated with this article can be found, in the online version, at doi:10.1016/j.neuroimage.2026.121870.

References

Antons, M., Lindner, M., Grosch, M., Oos, R., et al., 2022. Longitudinal [18]UCB-H/[18F] FDG Imaging depicts complex patterns of structural and functional neuroplasticity following bilateral vestibular loss in the rat. Sci. Rep. 12, 6049. https://doi.org/10.1038/s41598-022-09936-w.

Ashburner, J., 2007. A fast diffeomorphic image registration algorithm. Neuroimage 38 (1), 95–113. https://doi.org/10.1016/j.neuroimage.2007.07.007.
Beckmann, C.F., Smith, S.M., 2004. Probabilistic independent component analysis for functional magnetic resonance imaging. IEEE Trans. Med. Imaging 23 (2), 137–152. https://doi.org/10.1109/TMI.2003.822821. PMID: 14964560.
Bense, S., Deutschländer, A., Stephan, T., Bartenstein, P., et al., 2004. Preserved visual-vestibular interaction in patients with bilateral vestibular failure. Neurology 63, 122–128. https://doi.org/10.1212/01.WNL.0000129545.79566.6A.
Boegle, R., Stephan, T., Ertl, M., Glasauer, S., Dieterich, M., 2016. Magnetic vestibular stimulation modulates default mode network fluctuations. Neuroimage 127, 409–421. https://doi.org/10.1016/j.neuroimage.2015.11.065.
Boegle, R., Ertl, M., Stephan, T., Dieterich, M., 2017. Magnetic vestibular stimulation influences resting-state fluctuations and induces visual-vestibular biases. J. Neurol. 264 (5), 999–1001. https://doi.org/10.1007/s00415-017-8447-6.
Boegle, R., Kirsch, V., Gerb, J., Dieterich, M., 2020. Modulatory effects of magnetic vestibular stimulation on resting-state networks can be explained by subject-specific orientation of inner-ear anatomy in the MR static magnetic field. J. Neurol. 267 (Suppl 1), 91–103. https://doi.org/10.1007/s00415-020-09957-3.
Bosmans, J., Gommeren, H., Mertens, G., Cras, P., et al., 2022. Associations of bilateral vestibulopathy with cognition in older adults matched with healthy controls for hearing status. JAMA Otolaryngol. Head Neck Surg. 148 (8), 731–739. https://doi.org/10.1001/jamaoto.2022.1303.
Bosmans, J., Gommeren, H., Zu Eulenburg, P., Gilles, A., Mertens, G., 2024. Is vestibular function related to human hippocampal volume? J. Vest. Res. 34 (1), 3–13. https://doi.org/10.3233/VES-230076.
Brandt, T., Dieterich, M., 2019. Thalamocortical network: a core structure for integrative multimodal vestibular functions. Curr. Opin. Neurol. 32 (1), 154–164. https://doi.org/10.1097/WCO.0000000000000638.
Brandt, T., Dieterich, M., Danek, A., 1994. Vestibular cortex lesions affect the perception of verticality. Ann. Neurol. 35, 403–412.
Brandt, T., Schautzer, F., Hamilton, D.A., Brüning, R., et al., 2005. Vestibular loss causes hippocampal atrophy and impaired spatial memory in humans. Brain 128, 2732–2741. https://doi.org/10.1093/brain/awh617.
Brown, E.C., Artigas, S.O., Elsner, S., Liu, L., Park, S.Q., 2025. Utilizing rewards to dampen fear and its recovery. Sci. Rep. 15, 17671. https://doi.org/10.1038/s41598-025-99758-3.
Couto-Ovejero, S., Ye, J., Kind, P.C., Till, S.M., Watson, T.C., 2023. Cerebellar contributions to fear-based emotional processing: relevance to understanding the neural circuits involved in autism. Front. Syst. Neurosci. 17, 1229627. https://doi.org/10.3389/fnsys.2023.1229627.
Cutfield, N.J., Scott, G., Waldman, A.D., Sharp, D.J., Bronstein, A.M., 2014. Visual and proprioceptive interaction in patients with bilateral vestibular loss. Neuroimage Clin. 4, 274–282. https://doi.org/10.1016/j.nicl.2013.12.013.
Cyran, C.A., Boegle, R., Stephan, T., Dieterich, M., Glasauer, S., 2016. Age-related decline in functional connectivity of the vestibular cortical network. Brain Struct. Funct. 221 (3), 1443–1463. https://doi.org/10.1007/s00429-014-0983-6.
Dieterich, M., Bauermann, T., Best, C., Stoeter, P., Schlindwein, P., 2007. Evidence for cortical visual substitution of chronic bilateral vestibular failure (an fMRI study). Brain 30, 2108–2116.
Dieterich, M., Bense, S., Lutz, S., Drzezga, A., Stephan, T., Bartenstein, P., Brandt, T., 2003. Dominance for vestibular cortical function in the non-dominant hemisphere. Cerebral Cortex 13 (9), 994–1007.
Dieterich, M., Kirsch, V., Brandt, T., 2017. Right-sided dominance of the bilateral vestibular system in the upper brainstem and thalamus. J. Neurol. 264 (1), 55–62. https://doi.org/10.1007/s00415-017-8453-8.
Dobbels, B., Mertens, G., Gilles, A., Claes, A., et al., 2019. Cognitive function in acquired bilateral vestibulopathy: a crosssectional study on cognition, hearing, and vestibular loss. Front. Neurosci. 13, 340. https://doi.org/10.3389/fnins.2019.00340.
Dordevic, M., Sulzer, S., Barche, D., Dieterich, M., Arens, C., Müller, N.G., 2021. Chronic, mild vestibulopathy leads to defeicits in spatial tasks that rely on vestibular input while leaving other cognitive functions and brain volumes intact. Life 11 (12), 1369. https://doi.org/10.3390/life11121369.
Fink, G., Marshall, J.C., Weiss, P.H., Stephan, T., et al., 2003. Performing allocentric visuospatial judgements with induced distorsion of the egocentric reference frame: an fMRI study with clinical implications. Neuroimage 20 (3), 1505–1517. https://doi.org/10.1016/j.neuroimage.2003.07.006.
Gaser, C., Dahnke, R., Thompson, P.M., Kurth, F., Luders, E., 2024. The Alzheimer's Disease Neuroimaging Initiative. CAT: a computational anatomy toolbox for the analysis of structural MRI data. Gigascience 13. https://doi.org/10.1093/gigascience/giae049 giae049.
Göttlich, M., Jandl, N.M., Sprenger, A., Wojak, J.F., et al., 2016. Hippocampal gray matter volume in bilateral vestibular failure. Hum. Brain Mapp. 37, 1998–2006. https://doi.org/10.1002/hbm.23152.
Göttlich, M., Jandl, N.M., Wojak, J.F., Sprenger, A., et al., 2014. Altered resting-state functional connectivity in patients with chronic bilateral vestibular failure. Neuroimage Clin. 4, 488–499. https://doi.org/10.1016/j.nicl.2014.03.003.
Grüsser, O.J., Pause, M., Schreiter, U., 1990a. Localization and responses of neurons in the parieto-insular vestibular cortex in the awake monkeys (*Macaca fascicularis*). J. Physiol. 430, 537–557.
Grüsser, O.J., Pause, M., Schreiter, U., 1990b. Vestibular neurons in the parieto-insular vestibular cortex of monkeys (*Macaca fascicularis*): visual and neck receptor responses. J. Physiol. 430, 559–583.
Guan, S., Wan, D., Zhao, R., Canario, E., Meng, C., Biswa, l B.B., 2023. The complexity of spontaneous brain activity changes in schizophrenia, bipolar disorder, and ADHD was examined using different variations of entropy. Hum. Brain Mapp. 44 (1), 94–118. https://doi.org/10.1002/hbm.26129.
Guldin, W.O., Grüsser, O.J., 1998. Is there a vestibular cortex? Trends Neurosci. 21, 254–259.
Halmagyi, G.M., Chen, L., MacDougall, H.G., Weber, K.P., McGarvie, L.A., Curthoys, I.S., 2017. The video head impulse test. Front. Neurol. 8, 258.
Hüfner, K., Binetti, C., Hamilton, D.A., Stephan, T., et al., 2011b. Structural and functional plasticity of the hippocampal formation in professional dancers and slackliners. Hippocampus 21 (8), 855–865.
Hüfner, K., Strupp, M., Smith, P., Brandt, T., Jahn, K., 2011a. Spatial separation of visual and vestibular processing in the human hippocampal formation. Ann. N. Y. Acad. Sci. 1233, 177–186. https://doi.org/10.1111/j.1749-6632.2011.06115.x.
Hwang, K., Bertolero, M.A., Liu, W.B., D'Esposito, M., 2017. The human thalamus is an integrative hub for functional brain networks. J. Neurosci. 37, 5594–5607.
Janzen, J., Schlindwein, P., Bense, S., Bauermann, T., Vucurevic, G., Stoeter, P., Dieterich, M., 2008. Neural correlates of hemispheric dominance and ipsilaterality within the vestibular system. Neuroimage 42 (2), 1508–1518.
Jelitai, M., Puggioni, P., Ishikawa, T., et al., 2016. Dendritic excitation–inhibition balance shapes cerebellar output during motor behaviour. Nat. Commun. 7, 13722. https://doi.org/10.1038/ncomms13722.
Jia, X.Z., Sun, J.W., Ji, G.J., Liao, W., et al., 2020. Percent amplitude of fluctuation: a simple measure for resting-state fMRI signal at single voxel level. PLoS One 15 (1), e0227021. https://doi.org/10.1371/journal.pone.0227021.
Jongkees, L.B, Maas, J.P., Philipszoon, A.J., 1962. Clinical nystagmography. A detailed study of electro-nystagmography in 341 patients with vertigo. Pract. Otorhinolaryngol. 24, 65–93.
Judd, E.N., Lewis, S.M., Person, A.L., 2021. Diverse inhibitory projections from the cerebellar interposed nucleus. Elife 10, e66231. https://doi.org/10.7554/eLife.66231.
Kalisch, R., Wiech, K., Critchley, H.D., Dolan, R.J., 2006. Levels of appraisal: a medial prefrontal role in high-level appraisal of emotional material. Neuroimage 30, 1458–1466.
Kelly, R.M., Strick, P.L., 2003. Cerebellar loops with motor cortex and prefrontal cortex of a nonhuman primate. J. Neurosci. 23, 8432–8444. https://doi.org/10.1523/JNEUROSCI.23-23-08432.2003.
Kirsch, V., Boegle, R., Keeser, D., Kierig, E., et al., 2018. Handedness-dependent functional organizational patterns within the bilateral vestibular cortical network revealed by fMRI connectivity based parcellation. Neuroimage 178, 224–237. https://doi.org/10.1016/j.neuroimage.2018.05.018.
Kremmyda, O., Hüfner, K., Flanagin, V.L., Hamilton, D.A., et al., 2016. Beyond dizziness: virtual navigation, spatial anxiety and hippocampal volume in bilateral vestibulopathy. Front. Hum. Neurosci. 10, 139. https://doi.org/10.3389/fnhum.2016.00139.
Laux, L., Glanzmann, P., Schaffner, P., Spielberger, C.D., 1981. Das State-Trait Angstinventar (STAI). Theoretische Grundlagen und Handanweisung. Beltz, Weinheim.
Lee, E.S., Weon, Y.C., Kim, J.S., Lee, T.K., Park, J.Y., 2023. Functional and anatomical alterations in bilateral vestibulopathy: A multimodal neuroimaging study and clinical correlation. Front. Neurol. 14, 1157931. https://doi.org/10.3389/fneur.2023.1157931.
Liu, D., Yan, C., Ren, J., Yao, L., Kiviniemi, V.J., Zang, Y., 2010. Using coherence to measure regional homogeneity of resting-state FMRI signal. Front. Syst. Neurosci. 4, 24. https://doi.org/10.3389/fnsys.2010.00024.
Lopez, C., Blanke, O., Mast, F.W., 2012. The vestibular cortex in the human brain revealed by coordinate-based activation likelihood estimation meta-analysis. Neuroscience 60, 162–169.
Lotze, M., Klepzig, K., Stephan, T., Domin, M., Brandt, T., Dieterich, M., 2025. Overlaps of fMRI activation patterns of the anxiety-emotional and the vestibular-sensory networks. Neuroimage 315, 121275. https://doi.org/10.1016/j.neuroimage.2025.121275.
McCarthy, B., Datta, S., Sesa-Ashton, G., Wong, R., et al., 2023. Top-down control of vestibular inputs by the dorsolateral prefrontal cortex. Exp. Brain Res. 241, 2845–2853.
McCarthy, B., Rim, D., Sesa-Ashton, G., Crawford, L.S., et al., 2025. Electrical stimulation of the dorsolateral prefrontal cortex inhibits vestibular signalling in humans: A BOLD fMRI study. Brain Stimul 18 (3), 627–639.
Medina, J.F., Christopher Repa, J., Mauk, M.D., LeDoux, J.E., 2002. Parallels between cerebellum- and amygdala-dependent conditioning. Nat. Rev. Neurosci. 3, 122–131. https://doi.org/10.1038/nrn728.
Milad, M.R., Quirk, G.J., 2012. Fear extinction as a model for translational neuroscience. Ten years of progress. Annu. Rev. Psychol. 63, 129–151.
Neumann, N., Fullana, M.A., Radua, J., Brandt, T., Dieterich, M., Lotze, M., 2023. Common neural correlates of vestibular stimulation and fear learning: an fMRI meta-analysis. J. Neurol. 270 (4), 1843–1856. https://doi.org/10.1007/s00415-023-11568-7.
Nickerson, L.D., Smith, S.M., Öngür, D., Beckmann, C.F., 2017. Using dual regression to investigate network shape and amplitude in functional connectivity analyses. Front. Neurosci. 11, 115. https://doi.org/10.3389/fnins.2017.00115.
Oh, S.-Y., Nguyen, T.T., Kang, J.-J., Chae, J., Dieterich, M., 2025. Galvanic vestibular stimulation promotes visuospatial cognitive recovery in acute unilateral vestibulopathy via targeted neural modulation: a randomized controlled trial. J. Translat. Med. 23 (1), 991. https://doi.org/10.1186/s12967-025-07036-7.
Oh, S.-Y., Nguyen, T.T., Kang, J.-J., Kirsch, V., et al., 2023. Visuospatial cognition in acute unilateral peripheral vestibulopathy. Front. Neurol. 14, 1230495. https://doi.org/10.3389/fneur.2023.1230495.
Oldfield, R.C., 1971. The assessment and analysis of handedness: the Edinburgh inventory. Neuropsychologia 9 (1), 97–113. https://doi.org/10.1016/0028-3932(71)90067-4.

Popp, P., Wulff, M., Finke, K., Rühl, M., Brandt, T., Dieterich, M., 2017. Cognitive deficits in patients with a chronic vestibular failure. J. Neurol. 264, 554–563. https://doi.org/10.1007/s00415-016-8386-710:139.
Quirk, G.J., Mueller, D., 2008. Neural mechanism of extinction learning and retrieval. Neuropsychopharmacology 33, 56–72.
Richman, J.S., Moorman, J.R., 2000. Physiological time-series analysis using approximate entropy and sample entropy. Am. J. Physiol. Heart Circ. Physiol. 278 (6), H2039–H2049. https://doi.org/10.1152/ajpheart.2000.278.6.H2039.
Roberts, D.C., Marcelli, V., Gillen, J.S., Carey, J.P., Della Santina, C.C., Zee, D.S., 2011. MRI magnetic field stimulates rotational sensors of the brain. Curr. Biol. 21 (19), 1635–1640. https://doi.org/10.1016/j.cub.2011.08.029.
Schaefer, A., Kong, R., Gordon, E.M., Laumann, T.O., et al., 2018. Local-Global parcellation of the human cerebral cortex from intrinsic functional connectivity MRI. Cerebral Cortex 29, 3095–3114.
Schlindwein, P., Mueller, M., Bauermann, T., Brandt, T., Stoeter, P., Dieterich, M., 2008. Cortical representation of saccular vestibular stimulation: VEMPs in fMRI. Neuroimage 39 (1), 19–31.
Smith, P.F., 1997. Vestibular-hippocampal interactions. Hippocampus 7 (5), 465–471.
Smith, P.F., 2017. The vestibular system and cognition. Curr. Opin. Neurol. 30, 84–89. https://doi.org/10.1097/WCO.0000000000000403.
Smith, P.F., 2024. Aging of the vestibular system and its relationship to dementia. Curr. Opin. Neurol. 37 (1), 83–87. https://doi.org/10.1097/WCO.0000000000001231.
Smith, P.F., Darlington, C.L., Zhen, Y., 2015. The effects of complete vestibular deafferentation on spatial memory and the hippocampus in the rat: the Dunedin Experience. Multisens. Res. 28 (5-6), 461–485.
Smith, P.F., Horii, A., Russell, N., Bilkey, D.K., et al., 2005. The effects of vestibular lesions in hippocampal function in rats. Prog. Neurobiol. 75 (6), 391–405.
Sokunbi, M.O., 2014. Sample entropy reveals high discriminative power between young and elderly adults in short fMRI data sets. Front. Neuroinform. 8, 69. https://doi.org/10.3389/fninf.2014.00069.
Strupp, M., Brandt, T., Dieterich, M., 2023. Vertigo and Dizziness: Common Complaints, 3. Edition. Springer, London.
Strupp, M., Kim, J.S., Murofushi, T., Straumann, D., et al., 2017. Bilateral vestibulopathy: diagnostic criteria consensus document of the Classification Committee of the Bárány Society. J. Vestib. Res. 27, 177–189. https://doi.org/10.3233/VES-170619.
Turk-Browne, N.B., 2019. The hippocampus as a visual area organized by space and time: a spatiotemporal similarity hypothesis. Vision Res. 165, 123–130.
Von Neumann, J., Kent, R.H., Bellinson, R.H., Hart, B.I., 1941. The mean square successive difference. Ann. Math. Stat. 12 (2), 153–162. https://doi.org/10.1214/aoms/1177731746.
Wijesinghe, R., Protti, D.A., Camp, A.J., 2015. Vestibular interactions in the thalamus. Front. Neural Circuits 9, 79. https://doi.org/10.3389/fncir.2015.00079.
Xing, Y., Si, L., Wang, Y., Zhang, W., Ling, X., Yang, X., 2024. Altered functional connectivity of the multisensory vestibular cortex in patients with chronic unilateral vestibulopathy. Brain Connect. 14 (4), 252–259. https://doi.org/10.1089/brain.2023.0074.
Yang, A.C., Huang, C.C., Liu, M.E., Liou, Y.J., et al., 2014. The APOE ε4 allele affects complexity and functional connectivity of resting brain activity in healthy adults. Hum. Brain Mapp. 35 (7), 3238–3248. https://doi.org/10.1002/hbm.22398.
Yang, H., Long, X.Y., Yang, Y., Yan, H., et al., 2007. Amplitude of low frequency fluctuation within visual areas revealed by resting-state functional MRI. Neuroimage 36 (1), 144–152. https://doi.org/10.1016/j.neuroimage.2007.01.054.
Yeo, B.T.T, Krienen, F.M., Sepulcre, J., Sabuncu, M.R., et al., 2011. The organization of the human cerebral cortex revealed by intrinsic functional connectivity. J. Neurophysiol. 106 (3), 1125–1165.
Zang, Y., Jiang, T., Lu, Y., He, Y., Tian, L., 2004. Regional homogeneity approach to fMRI data analysis. Neuroimage 22 (1), 394–400. https://doi.org/10.1016/j.neuroimage.2003.12.030.
Zang, Y.F., He, Y., Zhu, C.Z., Cao, Q.J., et al., 2007. Altered baseline brain activity in children with ADHD revealed by resting-state functional MRI. Brain Dev. 29 (2), 83–91. https://doi.org/10.1016/j.braindev.2006.07.002.
Zheng, Y., Balabhadrapatruni, S., Baek, J.H., Chung, P., et al., 2012. The effects of bilateral vestibular loss on hippocampal volume, neuronal number, and cell proliferation in rats. Front. Neurol. 3, 20.
Zheng, Y., Goddard, M., Darlington, C.L., Smith, P.F., 2009. Long-term deficits on a foraging task after bilateral vestibular deafferentiation in rats. Hippocampus 19 (5), 480–486.
Zou, Q.H., Zhu, C.Z., Yang, Y., Zuo, X.N., et al., 2008. An improved approach to detection of amplitude of low-frequency fluctuation (ALFF) for resting-state fMRI: fractional ALFF. J. Neurosci. Methods 172 (1), 137–141. https://doi.org/10.1016/j.jneumeth.2008.04.012.
Zu Eulenburg, P., Caspers, S., Roski, C., Eickhoff, S.B., 2012. Meta-analytical definition and functional connectivity of the human vestibular cortex. NeuroImage 60, 162–169.